Rigidity transition in polymer melts with van der Waals interaction

Matthew L. Wallace and Béla Joós*
Ottawa-Carleton Institute for Physics, University of Ottawa Campus, Ottawa, Ontario, Canada K1N 6N5

Michael Plischke
Department of Physics, Simon Fraser University, Burnaby, British Columbia, Canada V5A 1S6
(Received 3 February 2004; revised manuscript received 16 July 2004; published 28 October 2004)

We study the onset of rigidity near the glass transition (GT) in a short-chain polymer melt modelled by a bead-spring model, where all beads interact with Lennard-Jones potentials. The properties of the system are examined above and below the GT. In order to minimize high-cooling-rate effects and computational times, equilibrium configurations are reached via isothermal compression. We monitor quantities such as the heat capacity C_P, the short-time diffusion constants $\mathcal{D}$, the viscosity η, and the shear modulus; the time-dependent shear modulus $G(t)$ is compared with the shear modulus μ obtained from an externally applied instantaneous shear. We give a detailed analysis of the effects of such shearing on the system, both locally and globally. It is found that the polymeric glass displays long-time rigid behavior only below a temperature T_1, where $T_1 < T_G$. Furthermore, the linear and nonlinear relaxation regimes under applied shear are discussed.

DOI: 10.1103/PhysRevE.70.041501 PACS number(s): 64.70.Pf, 61.25.Hq, 66.20.+d, 65.60.+a

I. INTRODUCTION

The onset of rigidity in disordered systems has been the focus of a number of studies over the last decades [1,2]. At the rigidity transition, a resistance to shear emerges, characterized by a nonzero shear modulus (above the transition), and a diverging viscosity (below the transition). In an important class of systems the onset of rigidity can be understood in terms of percolation [1,3–9]. Connectivity percolation coincides with the onset of an entropic component to rigidity [4–6], of the type traditionally associated with rubber [10]. Mechanical rigidity requires a rigid percolating backbone. If the interaction forces are central this means a multiply connected backbone, and consequently rigidity would appear at a higher concentration of bonds than connectivity percolation [11]. This physical picture provides a well-defined approach to understanding the behavior of the viscosity and the shear modulus in the neighborhood of the onset of entropic rigidity, and has been the focus of several recent studies [4–9]. The onset of the mechanical rigidity arising from covalent bonds has been extensively studied in network glasses at temperatures well below the glass transition (GT). In a mean-field argument, this component of rigidity sets in when the density of floppy modes approaches zero, or the number of constraints exceeds the number of degrees of freedom. For bond-bending networks, this means a mean coordination number $\langle r \rangle = 2.4$ [12–16].

In this paper we consider the onset of rigidity in a polymer melt which occurs as the temperature is lowered below the GT. There is no obvious length scale emerging *a priori* as the chains bind together under the attractive van der Waals interactions between monomers forming disordered structures. As we shall see, the region around the glass transition, where the viscosity is expected to diverge and a finite shear modulus to emerge, becomes more complex than in percolation driven systems. Where precisely the onset of rigidity occurs is an open question [15]. There is a body of literature on the behavior of the viscosity near the glass transition which will be used to discuss our results. There is, however, much less information about the onset of rigidity as measured by the emergence of a shear modulus.

The article proceeds as follows. Section II provides some general, conceptual background information regarding the GT, and in particular the behavior of the viscosity. Section III discusses our model and the computational tools that we have used. Section IV presents the main results obtained from these simulations and some brief explanations. In addition to the viscosity and the shear modulus we have calculated a short-time diffusion constant and the heat capacity. Section V, before the Conclusion, discusses the results within the current framework of polymeric glasses and provides some insight into the theoretical concepts discussed.

II. RIGIDITY AND THE GLASS TRANSITION

For a polymer melt, in contrast to the rigidity that sets in with increasing cross-link density, lowering the temperature drives the system reversibly toward a homogeneous glass phase with no obvious diverging length scale. Attempts have been made to invoke the percolation of the slow regions near the glass transition [17,18]. Also, in a particular model where rigid bonds can be formed upon cooling, a link is made to a mechanical rigidity transition based on constraint counting [19,20]. We will focus on the behavior of the viscosity and the shear modulus and analyze their critical behavior in a simple numerical model of a polymer melt made of short freely jointed chains. Discussions will be made using existing models of the physical properties of the system near the glass transition.

Historically viscosity has played an important role in analyzing glasses. The glass transition was associated for prac-

*Electronic address: bjoos@uottawa.ca

tical purposes with a specific number for the viscosity: $\eta = 10^{13}$ poise or 10^{12} Pa s, where the material could be considered not to flow during experimental time scales.

The glass transition is known as a "pseudo-second-order transition," since the discontinuities are not sharp and occur over a range of temperatures [21]. As well, a glassy system is not actually in equilibrium, because aging phenomena and flow have a non-negligible effect at long times. At best, we refer to a metastable equilibrium which, on our time scales (as in the case of short experimental times), can be treated as an equilibrium system.

A commonly used approach to the glass transition has been mode-coupling theory (MCT), derived from microscopic density fluctuations within a liquid [22,23]. A dynamic phase transition is predicted at approximately 1.1–1.3 times T_G, involving a divergence in the zero shear-rate viscosity η,

$$\eta = (T - T_{MC})^{-s}, \tag{1}$$

which could be masked by thermal activation effects [24]. More importantly, idealized MCT (which does not take into account "hopping" processes, for instance) predicts an ergodicity breaking at $T = T_{MC}$ [22]. It has also been proposed that there is, in fact, some type of "crossover point" to the Vogel-Fulcher-Tamman (VFT) regime (see [22] and references therein). The latter is a more successful framework for analyzing glass-forming liquids and is defined by the VFT law, an empirical equation of the form

$$\eta = \eta_\infty \exp\left(\frac{E_{act}}{T - T_0}\right). \tag{2}$$

The VFT temperature T_0 is expected and has been observed to be very close to the Kauzmann temperature T_K discussed in Refs. [22,25]. T_K is the temperature which defines a hypothetical state with zero configurational entropy or the formation of an "ideal" glass. Such a state is never reached because of the large slowing down of the system at T_G. Impressive fits to the VFT equation have been achieved [26,27] above the glass transition. These fits also provide a means to characterize the fragility of glasses: the closer T_G is to T_0 the more fragile the glass [28,29]. Nevertheless, the range of applicability of the VFT equation is under contention; some research indicates that it cannot go as low as T_G, while other studies suggest that it is best applied close to the GT (see Ref. [25] for a review).

A dynamical scaling approach was recently proposed to explain the divergence in relaxation time below the GT [28]. The GT is characterized by dynamical heterogeneity, in that only some of the material is able to move due to a lack of free volume. At a critical temperature T_C, there is not enough free volume for any particles to move and local motion is effectively prohibited. This approach assumes percolation-like universal behavior among glass-forming liquids with an additional activation energy term of the following form:

$$\eta \sim \left(\frac{T - T_C}{T_C}\right)^{-9} \exp\left(\frac{E}{kT}\right). \tag{3}$$

Unlike the MCT approach, the above equation yields a critical temperature for viscosity divergence T_C below T_G. While experimental data from polymeric liquids are well described without the activation energy contribution, the extra term ensures the same universality class for all glass formers [28].

One can also consider the GT in terms of the "energy landscape" of the system, a hypersurface punctuated by local minima of varying depth, where the shape depends on the volume and the sampling on the temperature [21,25,30,31]. In terms of energy, T_G can be seen as a temperature at which the system is "trapped" in a relatively deep local minimum and the free energy barriers effectively prevent further exploration of phase space. Polymeric glasses do not behave like other, more simple glasses, such as SiO_2. Simple glasses have a more precisely defined energy landscape, whereas polymeric glasses have more configurational possibilities, yielding more local minima which can be sampled via local rearrangements. As such, polymers tend to create relatively "fragile" glasses, characterized by a non-Arrhenius variation of the viscosity with temperature. In terms of the glass transition temperature, it has been observed that T_G rises with chain length or molecular weight until a plateau around $M = 100$ [24].

In general, glasses display a more complex response to low-frequency shearing than purely elastic systems. Nonlinear mechanical responses are common in glass systems after ergodicity breaking [25], and the relaxation of a simple glass will depend on local rearrangement. In polymer systems there is an additional component arising from the extension of the chains. This, as well as energy landscapes, will be useful tools in interpreting the mechanical response within our glassy polymer melt. Some aspects of relaxation below the GT are well understood [25,32] in terms of aging subsequent to a temperature quench or in response to a mechanical deformation, after which glasses can relax fairly quickly. However, this has not, to our knowledge, been examined using an instantaneous simple shear experiment.

III. MODEL

A. The bead-spring model

We have used the well-known bead-spring model based on work by Kremer and Grest [33] and more recently applied with success by the research group of Binder *et al.* [22,26,34–36]. Their work has focused on issues such as α and β relaxation, cooling-rate dependencies, and cage effects on approaching T_G from above. In this model, the neighboring beads along each chain (there are ten monomers per chain and a total of $N = 1050$ monomers) interact through the finitely extensible nonlinear elastic (FENE) potential

$$U_{FENE}(r_{ij}) = \frac{1}{2} k R_0^2 \ln\left[1 - \left(\frac{r_{ij}}{R_0}\right)^2\right] \tag{4}$$

where $R_0 = 1.5$, $k = 30$. In addition, all particles interact though the truncated Lennard-Jones potential,

$$U_{LJ}(r_{ij}) = 4\varepsilon_{LJ}\left[\left(\frac{\sigma}{r_{ij}}\right)^{12} - \left(\frac{\sigma}{r_{ij}}\right)^{6}\right] + C, \quad r_{ij} < 2.5\sigma, \quad (5)$$

where C is chosen such that the potential is zero at the cutoff radius.

The length is rescaled using $\sigma=1$ and the temperature is expressed in units of ε_{LJ}/k_B. Combining the two potentials yields an optimum bond length of 0.96σ, which inhibits crystallization by introducing a competing length scale.

B. Approaching the glass phase along an isotherm

Usually the GT is approached at constant P by lowering the temperature [26,34–37]. In order to avoid problems associated with high cooling rates [36] and to reduce computational time, we propose a method whereby the samples can be "frozen" or not, as the case may be, by compression at a desired T. Although we are still measuring changes in a given quantity with respect to temperature with a constant pressure, we are effectively using a different thermodynamic path to define the state of a sample. There is a very complete discussion of thermodynamic paths in Ref. [37]. However, it does not discuss defining a thermodynamic state using an isothermal path. Our method seems to allow a better exploration of phase space and, consequently, a more physically meaningful final state for low temperatures. In a pure Lennard-Jones simulation, for instance, we found that crystallization requires less CPU time when compressing the system than when simply cooling it [38]. The temperatures studied range from $1.2\epsilon_{LJ}/k_B$ to $0.2\epsilon_{LJ}/k_B$, allowing us to explore the liquid, supercooled, and glassy regimes. We entered the glass phase along both an isochore and an isobar. However, we retained only the simulation results along the isobar, as pressure variations along the isochore proved somewhat unphysical. The main problem was a progressive increase of pressure with lowering temperature below T_G (similar results were found in Ref. [35]). This discrepancy effectively amounts to

$$\left(\frac{\partial P}{\partial T}\right)_{N,V} = \frac{T}{V}\left(\frac{\partial S}{\partial T}\right)_{N,V} < 0 \quad (6)$$

which is clearly forbidden. Along the constant volume path, the system goes through what would have been a two-phase region in the thermodynamic limit.

For a given sample, we create an initial "gas" of polymers at the desired temperature, having ensured their separation and random orientations. The chains reach their individual equilibrium configurations in an *NVT* ensemble using an algorithm based on the Langevin equation, called Brownian dynamics (BD) in Ref. [39]:

$$m\frac{d^2x_i}{dt^2} = -\frac{\partial U_i}{\partial x_i} + m\Gamma\frac{dx_i}{dt} - W_i(t). \quad (7)$$

This algorithm allows the system to reach equilibrium in our "expanded" volume quickly and realistically, by simulating a heat bath in the form of a friction coefficient Γ and by introducing a random force W in the form of Gaussian noise. Subsequently, the system is compressed to the pressure $P=1.0\epsilon_{LJ}/\sigma^3$ to achieve a similar system to that of Binder's research group [26,34–37]. The compression is done in the BD *NVT* ensemble by reducing affinely the system size at a specified rate. The largest compression rate of a side of the box, in Lennard-Jones units, was around $0.015\sqrt{\varepsilon_{LJ}/m}$. Using a smaller compression rate was shown to cause negligible change in quantities such as viscosity and energy. Naturally, the rate of compression will inevitably have some effect on determining at what temperature T_G the glass becomes "stuck." However, we believe that, by continuously changing the volume (and thus the precise shape of the energy landscape), the system can eventually find a lower energy minimum. The final volume is established at a given temperature for $P=1$ using a constant pressure damped-force algorithm [39]. The system is then allowed to evolve in a microcanonical ensemble by molecular dynamics (MD). We need to run in that ensemble to collect information on the correlators required to calculate viscosity and shear modulus related quantities. The equations of motion were integrated with the standard velocity Verlet algorithm [39] and a time step of $dt=0.005\sqrt{m\sigma^2\varepsilon_{LJ}}$. During this portion of the simulation, both the pressure and the temperature were seen to fluctuate around their expected values.

C. Viscosity and shear modulus from the stress autocorrelation function

The time-dependent shear modulus $G(t)$ measures the response of the system to a shear strain $\epsilon_{\alpha\beta}$ applied at $t=0$, and is defined as [10]

$$G(t) = \frac{\sigma_{\alpha\beta}(t)}{\epsilon_{\alpha\beta}}, \quad \alpha \neq \beta. \quad (8)$$

$\sigma_{\alpha\beta}$ is an off-diagonal macroscopic stress tensor element and implicitly includes inter- and intrachain interactions. $G(t)$ can be calculated from the stress fluctuations in the quiescent melt using the fluctuation dissipation theorem which states that [10]

$$G(t) = \frac{V}{kT}\langle\sigma_{\alpha\beta}(t_0)\sigma_{\alpha\beta}(t_0+t)\rangle, \quad \alpha \neq \beta, \quad (9)$$

where

$$\sigma_{\alpha\beta} = -\frac{1}{V}\left(\sum_{i=1}^{N} m v_{i\alpha}v_{i\beta} - \sum_{i<j}^{N}\frac{r_{ij\alpha}r_{ij\beta}}{r_{ij}}\frac{\partial U_{ij}}{\partial r_{ij}}\right). \quad (10)$$

The sums are over all the particles in the system indexed from 1 to N. $G(t)$ is a very powerful tool: it allows us to obtain a zero-shear limit for the shear modulus without external deformation, which can have a non-negligible effect on the steady state. Nonergodic glassy materials are especially sensitive to configurational changes. Instead, $G(t)$ simply uses the microscopic density fluctuations and the subsequent response to give us a clear picture of how the stress evolves in a system. At $t\to\infty$, $G(t)$ becomes the "equilibrium modulus," G_{eq} and, at $t\to 0$, $G(t)$ becomes G_∞, the infinite-frequency modulus [40,41]. To our knowledge, G_{eq} has never been compared to the usual shear modulus, which is mea-

sured by a system's response to a shear deformation (see Sec. III E below). The zero-shear-rate viscosity is obtained by the appropriate Green-Kubo formula:

$$\eta = \int_0^\infty G(t)dt, \tag{11}$$

from which one can obtain the relaxation time as

$$\tau = \frac{\eta}{G_\infty}. \tag{12}$$

In the past, viscosity measurements have been made using nonequilibrium molecular dynamics (NEMD) to avoid the problem of long time tails of correlation functions at temperatures approaching T_G [27]. This issue was resolved by fitting $G(t)$ to the Kohlrausch-Williams-Watts (KWW) or stretched-exponential function and integrating to infinity, via [40]

$$G(t) = G(0)\exp\left[-\left(\frac{t}{t_0}\right)^\beta\right]. \tag{13}$$

The quality of the fits as well as previous research [25] suggest that this approach reflects well the behavior of the system over long time scales. Although there is a certain additional error associated with the fit, it allows us to keep a system in its "true," undriven state. The errors were large for T very close to T_G ($T \sim T_G + 0.02$), due to the increasing length of the tails.

The nature of the tail changes significantly below the glass transition, and the KWW fit of Eq. (13) is no longer appropriate. The slow relaxation of the glass through thermally activated processes is better represented by the power law form [40,41]

$$G(t) = G_{eq} + At^{-\varphi}. \tag{14}$$

In physical terms the power law fit uses the distribution of energy barriers explored by the system during the simulation time to predict the long-time behavior.

D. Short-time diffusion coefficients

To get an idea of the mobility of the chains and the individual particles, we define short-time diffusion coefficients using the Einstein relations, $\mathcal{D}_M$, for individual particles i, and $\mathcal{D}_{CM}$, for the centers of mass of individual chains j:

$$\mathcal{D}_M = \frac{\langle[\mathbf{r}_i(t) - \mathbf{r}_i(0)]^2\rangle}{6t}, \tag{15}$$

$$\mathcal{D}_{CM} = \frac{\langle[\mathbf{r}_j(t) - \mathbf{r}_j(0)]^2\rangle}{6t}. \tag{16}$$

Ignoring initial displacements, we simply retain the slope of the first approximately linear part of the mean-square displacement vs time graph, calculated around 30 000 dt. In the asymptotic limit if the particles are delocalized, there would be on a longer time scale a linear regime with a smaller slope. If they are localized, $(\langle\Delta r\rangle)^2$ will be bounded. In the liquid phase, the first linear regime essentially reflects the local diffusion of a particle, which is limited by the proximity to its neighbors. In the glassy regime, there may be little or no diffusive behavior. Nevertheless, the approximately constant slope is an indicator of how much local mobility a given monomer or chain can have within its cage.

E. The shear modulus from the shear deformation

We have also calculated the shear modulus directly by applying a simple shear deformation to a given sample. We start with a cube of side L. For a given strain ε_{xy}, an affine shear deformation in the x direction is applied (in a plane with its normal along the y direction). An atom initially in position (x,y,z) is displaced to $(x+\epsilon_{xy}y,y,z)$. The boundaries of the simulation box consequently are shifted for x_{min} from 0 to $\varepsilon_{xy}y$ and for x_{max} from L to $\varepsilon_{xy}y+L$. This is applied as a one-time, instantaneous deformation. The shear modulus is then calculated with an off-diagonal element of the stress tensor, once the system is equilibrated:

$$\mu = \frac{[\sigma_{xy}(\varepsilon_{xy}) - \sigma_{xy}(0)]}{\varepsilon_{xy}}. \tag{17}$$

The shearing is applied in the five other directions, substituting xy by yz, $-xy$, etc. Individual samples lack symmetry and therefore the various deformations will not usually give the same stress components. The evolution of the residual stress is monitored, until a stress plateau is reached in the deformed system. Deformations of $\varepsilon = 0.01$ to 0.2 were performed. A simple shear deformation is more rigorous than a pure shear deformation, which relies heavily on the assumption of isotropy throughout the system [5]. In a pure shear deformation, a sample would have been stretched along x by ε_{xy} resulting in a compression along the two other directions by $\varepsilon_{xy}/2$ in a volume preserving system.

F. Heat capacity

Finally, we monitored the changes in the heat capacity C_P across T_G. Although other methods exist for calculating C_P via MD simulations, the best approach was to calculate the potential energy in the *NVT* ensemble (Brownian dynamics) for each temperature. Knowing the volume and the pressure at each temperature, we can obtain the specific heat per particle C_P in units of k_B from

$$C_P = \frac{1}{N}\left(\frac{\partial H}{\partial T}\right)_{N,P}, \tag{18}$$

where $H = E + PV$ is the enthalpy.

G. The simulations

Most simulations were carried out on the "Bugaboo" Beowulf Cluster at Simon Fraser University, with computational times for one complete sample at a given temperature (*ab initio* and including all correlations and shearing) at around 6 days on a single processor. Approximately ten samples of 1050 particles are examined for each temperature, with each given sample being used to calculate approximately 400 "correlators" of length 30 000 dt.

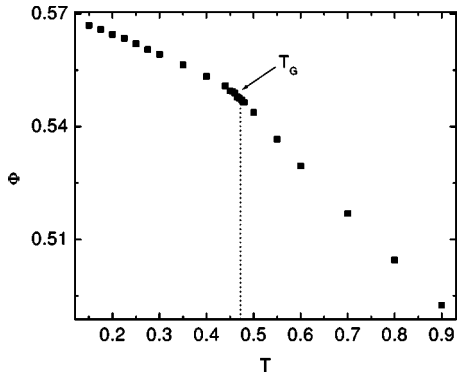

FIG. 1. Packing fraction Φ as a function of temperature. The intersection of the two slopes in the glassy and liquid regimes accurately determines T_G, shown with the arrow and dotted line.

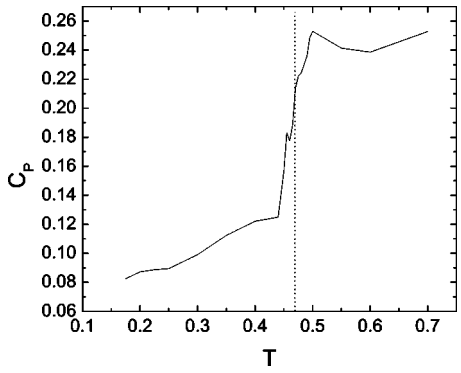

FIG. 2. Heat capacity C_P found by numerically deriving the enthalpy H with respect to temperature. The dotted line shows the location of T_G as determined from Fig. 1. Note that the drop in C_P as T is lowered ends at $T=0.44$, coinciding with the appearance of long-term rigidity (see Fig. 6).

IV. RESULTS

A. The glass transition temperature T_G

We begin by establishing the glass transition temperature T_G, using the common and accessible method (both experimentally and by simulation) of examining the volume (or equivalently, the packing fraction Φ) across the GT [10,42] along the isobar $P=1$. The intersection of the slopes in the solid and liquid regimes separates two regions of nearly constant volume expansivity. It yields an unambiguous value of $T_G=0.465\pm0.005$, as shown in Fig. 1 and Table I. The variation of C_P with respect to temperature provides another estimate. As discussed in Sec. III F, C_P was calculated from the derivative of the enthalpy with respect to temperature along an isobar (Fig. 2). Such an approach has been extensively used to calculate T_G and as expected, C_P is characterized by a sharp increase around T_G [21]. The increase, however, takes place over a temperature interval, and it is not clear what part of the curve should be used as the location of T_G (see Fig. 2). The start of the rapid rise occurs at 0.44 and ends at 0.50. The T_G determined above from the change in value of the volume expansivity lies in the middle of the rapid rise. The beginning of the rapid rise suggests that a major change in the entropy is taking place at that point. As we shall see later, this point has a special significance.

B. The viscosity

Now that we can identify the GT within our system, we can examine the relevant dynamical quantities around this point. First, we obtain the expected viscosity curve with the characteristic increase over several orders of magnitude around T_G, along with the corresponding curves of Eqs. (2) and (3) obtained using a simple nonlinear curve-fitting algorithm (Fig. 3). We also attempt a fit using the MCT approach in Eq. (1). The results are summarized in Table I and follow the same trends as those found in Refs. [22,35] for a similar system. The attractive Lennard-Jones [LJ] interaction has a shorter cutoff 2.24σ, instead of our 2.5σ, leading to systematically lower critical temperatures. Varnik and Binder [27] have looked at the increase in viscosity with lowering of the temperature in the same system but with the melt driven by a force field. The values of T_{MC} and T_0 are quite different under those conditions, expectedly lower.

We get an idea of fragility by plotting the logarithm of the viscosity η versus the inverse temperature, a characteristic T_G-scaled Arrhenius curve for glassy systems (Fig. 4). Evidence of fragility (deviations from Arrhenius behavior) becomes apparent as we approach the GT. Typical experimental data from polymeric glasses generally show very fragile behavior from such plots [25].

TABLE I. Relevant temperatures characterizing the glass and rigidity transitions: T_G is the glass transition with the associated MCT critical temperature T_{MC}, the VFT temperature T_0, and the critical temperature T_C obtained from Eq. (3). In addition, we present T_1, corresponding to the onset of true rigidity, found by extrapolation to G_{eq} in Eq. (14).

T_G	T_{MC}	T_0	T_C	T_1
0.465 ± 0.005	0.51 ± 0.02	0.41 ± 0.02	0.422 ± 0.006	0.44 ± 0.01

C. The shear modulus from $G(t)$

We have also examined how $G(t)$, the time-dependent shear modulus, changes as we cross the glass transition

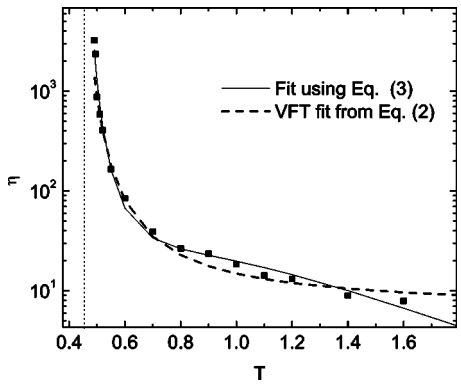

FIG. 3. Viscosity η above the glass transition, along with the corresponding fits from Eqs. (2) and (3). The dotted vertical line marks T_G obtained previously.

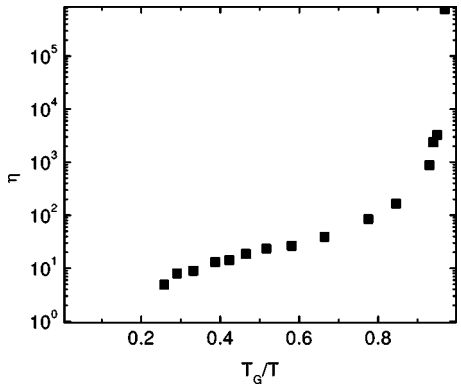

FIG. 4. Glassy behavior of the polymer melt shown in a typical Arrhenius plot, indicating that the glass is primarily fragile.

(Fig. 5). The main difference between solid and liquid regimes occurs in the long-time tails of $G(t)$. While a KWW fit of Eq. (13) can be used for $T>T_G$, a power law of the form of Eq. (14) must be applied for $T<T_G$ [40,41]. Simply evaluating the value of $G'_{eq}=G(t)$ at the end of our correlation function ($t=150\sqrt{m\sigma^2/\varepsilon}$) gives a good idea of the initial degree of relaxation possible in our system, or the shear modulus at short time scales. However, we would like to examine the "true," long-time relaxation of the glass, which is generally not accessible at simulation time scales. As such, we find G_{eq} (at $t\to\infty$) using a nonlinear fit to the power law of Eq.(14), giving nonzero values of G_{eq} beginning at $T_1=0.44\pm0.01$, and an approximately linear increase with decreasing temperature, as shown in Fig. 6. The decay of $G(t)$ is very slow, and most of the information necessary for the fit can be extracted from the initial decay region, shown in the inset of Fig. 5. Similar power law behavior has been found in colloidal gel simulations [41]. We are further convinced of this approach by the apparent change of slope of G'_{eq} at the point where G_{eq} becomes nonzero. G'_{eq} begins acquiring nonzero values at higher T (near $T_{MC}=0.51$, the idealized MCT temperature). In other words, apparently "solid" glasses can have an almost liquidlike response at longer times, provided the temperature is just above or just below T_G. This is perhaps due to some degree of nonergodicity in the system. We cannot put a precise value on the time scale of the long-term rigidity, only that it is much greater than that of the simulation.

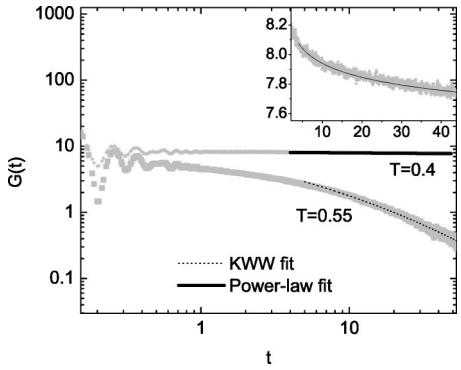

FIG. 5. Stress autocorrelation function $G(t)$ decay above and below T_G, as calculated from Eq. (9), along with the corresponding KWW and power-law fits from Eqs. (13) and (14). Note the very slow power law decay. Inset: Initial decay of the power law for $T=0.4$ shown on a linear plot.

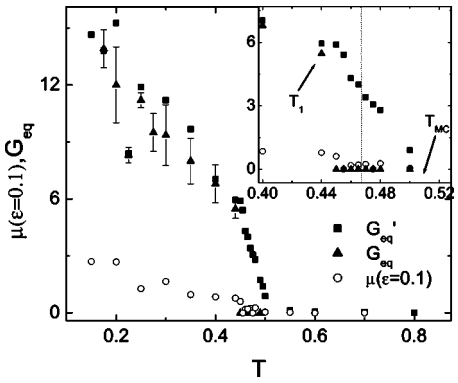

FIG. 6. Various approaches to determining the shear modulus. G'_{eq} is simply the value of $G(t)$ at $t=150$ time units (the rigidity on very short time scales), while G_{eq} is obtained by fitting the function to Eq. (14) at $t\to\infty$. Finally, μ is calculated from Eq. (17) via a non-negligible deformation of the sample. The inset shows the behavior around the GT (dotted line) with the locations of T_1 (the onset of long-term rigidity) and T_{MC} (the MCT temperature) indicated by arrows.

D. The shear modulus from a finite deformation

We also confirm our G_{eq} results by checking whether or not they represent the shear modulus μ in its regular sense, i.e., the response to a shear deformation. μ, the value of G'_{eq} on our short simulation time scales and the value of G_{eq} by fit are shown in Fig. 6. This preliminary comparison is promising, since both G_{eq} and $\mu(\varepsilon=0.1)$ begin acquiring nonzero values at the same temperature T_1 defined in the previous section: they are both good indicators of the onset of true rigidity. Clearly $\mu(\varepsilon=0.1)$ is much smaller than G_{eq}: while G_{eq} calculates the shear modulus via the internal fluctuations, μ requires external constraints to be imposed, thus altering the system. As such, we look for the limit $\mu(\varepsilon\to0)$. Figure 7 shows the function $\mu(\varepsilon)$ for a set of samples at three given temperatures. This calculation was done by ensuring that the stress had reached a plateau before evaluating μ, via Eq. (17) . Clearly, this glass displays highly nonlinear behavior and we have, as of yet, no function with which to fit the points. The limit $\varepsilon\to0$ is computationally prohibitive to reach. The error in μ as seen from Eq. (17) grows as $1/\epsilon$. Figure 7 does, however, indicate that $\mu(\epsilon\to0)$ likely tends to G_{eq}. It also suggests that the regime of elastic deformation for these glasses is approximately 2–3 %.

E. The short-time diffusion coefficients

To gain more insight into the structural behavior of the melt near the glass transition we look at the short-time diffusion coefficients $\mathcal{D}_M$ and $\mathcal{D}_{CM}$ of the monomers and center of mass of chains respectively, defined in Sec. III D. The measurements reflect, on average, how much local motion is

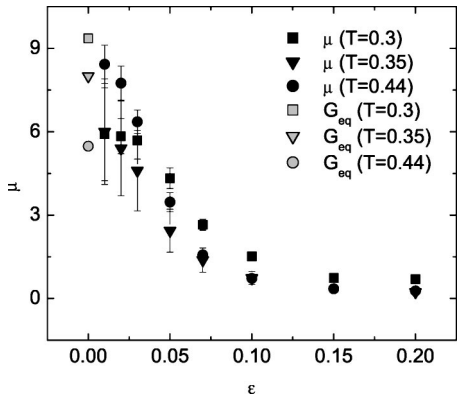

FIG. 7. Shear modulus μ as a function of shear for three temperatures below the GT. We interpret the G_{eq} as the zero-shear limit to check whether these two methods agree. Note how the statistics get much worse at small ε.

possible for a given particle. As expected, as we decrease the temperature, there is decreased local diffusion as we approach the rigidity transition and GT (see Fig. 8). In addition we notice that, in the glassy regime, the monomers maintain significantly more short-time mobility than the chains close to T_G. The chains, on the other hand, are more constrained. This is further illustrated by the behavior of the ratio $\mathcal{D}_M/\mathcal{D}_{CM}$ with temperature. Figure 9 reveals that monomer motion becomes increasingly dominant as we approach T_G from above. There could be enough free volume for some monomers to move short distances [28]. This has been illustrated by the cage effect [34]: as the chains become immobilized near T_G, the monomers maintain some degree of mobility within their "cage" formed by the neighbors. This is, in fact, an important precursor to the system becoming not only "slow," but also rigid. At T_G the monomers still have sufficient mobility to absorb deformations. This may explain why the onset of shear rigidity is below T_G.

V. DISCUSSION

We have determined the glass transition temperature for our system of freely jointed chains interacting with van der

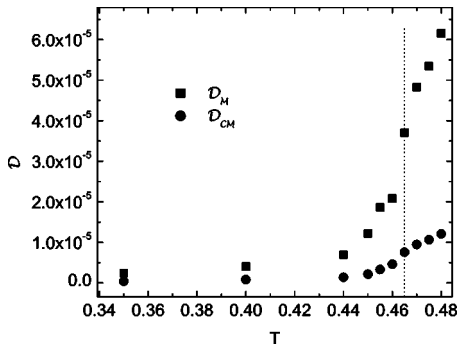

FIG. 8. Average short-time diffusion of monomers ($\mathcal{D}_M$) and centers of mass of chains ($\mathcal{D}_{CM}$) around T_G. The substantial increase in $\mathcal{D}_M$ begins slightly below T_G (indicated by the dotted line).

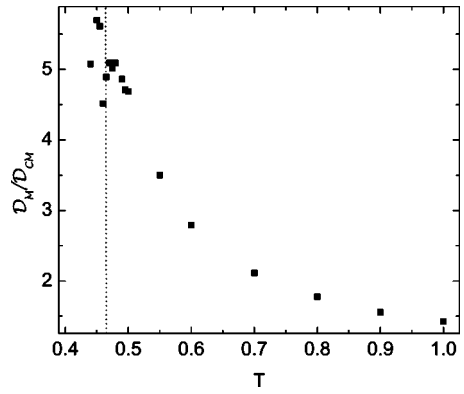

FIG. 9. Cage effect as seen by dividing the monomer by the chain diffusion constants at short times. The maximum occurs near T_G (dotted line), as the cage progressively "closes in."

Waals interactions through the change of slope of the packing fraction with temperature, or the change in the value of the volume expansivity. This led to a value of $T_G = 0.465 \pm 0.005$. At the glass transition the heat capacity at constant pressure C_P exhibits a sharp rise with increasing temperature. The above determined T_G occurs in the middle of the rise. As seen in Table I a number of other temperatures have been obtained in our study of the onset of rigidity brought about by the kinetic arrest occurring near T_G. The beginning of the rise in C_P coincides with $T_1 = 0.44 \pm 0.01$ the point of onset of rigidity as measured by G_{eq} and μ, and the end of the rise with $T_{MC} = 0.51 \pm 0.02$, the MCT critical temperature, the divergence point in the viscosity predicted by mode-coupling theory. These coincidences do not appear fortuitous. The rapid rise in C_P suggests a temperature interval where the configuration space explored by the glass in the making changes rapidly. The end of the rise may very well be the temperature at which thermally activated processes end and the assumptions of idealized MCT become valid. T_{MC} is expected to be higher than T_G [43]. Below T_{MC}, the liquid can still flow with the help of thermally activated hops. The temperature of rigidity onset was determined by studying the behavior of the viscosity η and the shear modulus upon cooling. The divergence point of η is obtained by extrapolation, while the onset of rigidity is measured fairly close to the transition. So we will begin with the latter. At T_G by all indications the system has no long-time shear resistance. Both $G_{eq} = \lim_{t\to\infty} G(t)$ and μ, obtained by an actual deformation of the system, are still zero. $G'_{eq} = G(t \approx 150)$, the short-time shear modulus, becomes nonzero around T_{MC}. But G_{eq}, its long-time limit, only sets in at $T_1 = 0.44 \pm 0.01$. At the same temperature μ becomes nonzero, although the values of μ are not the same as those of G_{eq} for typical deformations of $\epsilon = 0.05$ or 0.1 (see Figs. 5 and 6). We will elaborate on these differences later in the discussion. The important point is that they agree on the temperature of rigidity onset. On the other hand, the divergence point of the viscosity η was determined using several models, two of which incorporate thermally activated processes, which become operative below T_{MC}. They predict divergences at $T_0 = 0.41 \pm 0.02$ from a fit to the VFT law [see Eq. (2)] and $T_C = 0.422 \pm 0.006$ from the Colby form [see Eq. (3)]. One

should, however, note that these are obtained by extrapolating from the lowest temperature at which η have been measured, 0.49. The true states at T_0 or T_C are not attained due to the dramatic slowing down below T_G. The extrapolated values are smaller than T_1, but not inconsistent with it. They are not expected to be as reliable because they are not measured directly. The fact that T_1 is smaller than T_G determined from the change in volume expansivity raises the question about the true location of the glass transition. Does this mean that the beginning of the rise in C_P should be used as the true onset of the glass transition, or is it that at T_G, although there is structural arrest, sufficient free volume remains to allow for small deformations at no cost of energy?

A number of aspects of this study are worth commenting on further. First there is always a time scale associated with rigidity, as it is well known that the shear response depends on frequency. What we are trying to determine is the static shear modulus, or zero frequency limit. The long time associated with this modulus, as measured, is still short compared with temperatures related to aging. We started measuring quantities when the system showed no sign of evolving. In other words, aging is on a different time scale than stress relaxation times. An unrelated issue on time scale is the definition itself of T_G which is linked to the experimental time scale. The glass makers, as mentioned in Sec. II, use a value of 10^{13} Pa s for the viscosity at T_G. This corresponds to the experimental time scale of minutes (or hours) [21] while a computer experiment, under the best of conditions, occurs over nanoseconds, so about 10^{11} smaller. It is intriguing to note that the VFT fit and the Colby fit yield viscosities at T_G of the order of 10^7 in our units, which with G_∞ of the order of 10^2 gives a relaxation time of the order of 10^5 at T_G, longer than the time scale of our computer experiments, closer to 10^4 time units or 10^6 time steps.

Another point is the nature of the onset of rigidity. What happens at T_1? Studies under way [44] show that the distribution of displacements on all time scales studied is unimodal as previously observed [45], so there is no separate long-lived rigid backbone that accounts for the resistance to applied shear. Second, the local structure of the system remains identical, as expected from a GT. In other words, there is no evidence of any clusters of tightly packed particles. The average distance to the nearest neighbors of a given particle does not change appreciably with temperature. The concept of dynamical heterogeneity may be more applicable to this system [45,46], in that the lack of mobile clusters on fairly long time scales below T_1 accounts for rigidity. Instead of having covalent bonding, the van der Waals rigidity in our system may arise from "jamming" constraints produced by mechanisms such as the cage effect, which relies primarily on the presence of stiff chains to prevent motion.

The fact that the appearance of long-term rigidity at $T_1 = 0.44$ coincides with the bottom of the characteristic "dip" in the heat capacity curve (Fig. 2) is indicative of an increase in system stability as the temperature is lowered. In network glasses, the number of floppy modes in the system determines the jump in C_P (also related to the fragility of the glass) [47]. And these floppy modes start appearing at T_1. Other approaches have been able to associate C_P with the change in entropy of constraint breaking [16]. Although these approaches rely on physical bonds as constraints, the same principles could apply to our system. Furthermore, we notice from Fig. 8 that $\mathcal{D}_{CM}$ is very small at T_1.

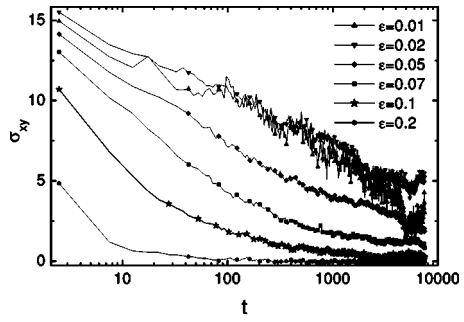

FIG. 10. Decay of the shear stress σ_{xy} after various initial shear deformations at $T=0.3$. We can see both the initial stress and the shape of the subsequent decay in the system. Note that for large ε there is very little initial stress imparted, followed by a fast decay.

Finally we would like to comment on the difference between G_{eq} and μ, the latter obtained from the application of an instantaneous simple shear to the system. The nonlinear behavior of Fig. 7 is further explained in Fig. 10. Both the initial stress and the degree of relaxation are highly dependent on ε (Fig. 10). For larger shearing, the initial stress is smaller and the subsequent decay is very fast. A collapse was realized by plotting the stress scaled to its initial value versus time scaled with a relaxation time equal to the time to reach half the stress. The relaxation times obtained follow the same trend as μ. The shearing is likely irreversible at large strain. In effect, large deformations appear to have a substantial effect on the structure of the system, perhaps changing the shape of the energy landscape and causing the system to be in a different local minimum. Small shear, however, does not generally have the same effect and a larger residual stress remains as the system tries to return to its original configuration (the same energy well). Having described the basic behavior associated with shearing, we can alternatively examine the local "polymeric" contribution to the mechanical relaxation of the glass. Considering Fig. 11, we can see that for small ε, the chains are slightly stretched, but can easily recover their equilibrium R_G value, where R_G is the average radius of gyration of the chains. For larger strains, the initial

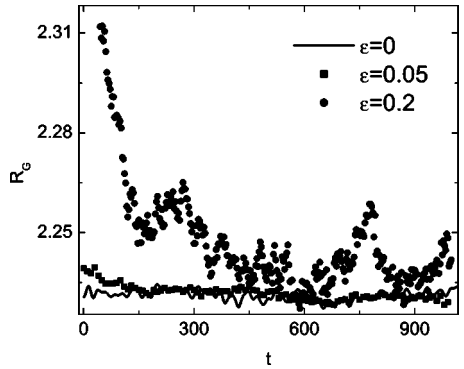

FIG. 11. Evolution of the average radius of gyration, R_G, of the polymer chains, after a large ($\epsilon=0.2$) and small ($\epsilon=0.05$) deformation at $t=0$ together with the undeformed, "equilibrium" R_G ($\epsilon=0$).

deformation of chains is disproportionately high and there can be no recovery on intermediate time scales. We can interpret the degree of recovery in the chain as the main factor characterizing the viscoelastic behavior in polymer melts (often represented by spring-dashpot models), since chain length has a direct, substantial effect on relaxation mechanisms. Because of the absence of permanent crosslinks, the chains slip during relaxation. For this reason the entropic contribution to rigidity is not dominant. This contribution is also intrinsically difficult to resolve with the degree of noise in the data. The rigidity observed in this system can be viewed as mainly mechanical. Finally, rigidity should occur earlier in a system of longer chains, since each particle will have, on average, fewer degrees of freedom.

VI. CONCLUSION

Our isothermal compression method has allowed us to better examine the state of the melt above and below T_G. Our studies of rigidity bring additional insight into the nature of the GT. Previous studies on structural issues related to the glass transition have focussed on the divergence of the viscosity. We provide an additional perspective by looking also at the emergence of the shear resistance. Whereas the point of divergence of the viscosity is difficult to assess directly because of structural arrest, it appears easier to approach the point of onset of the shear modulus. That both G_{eq} and μ have the same onset is encouraging. The work demonstrates the effectiveness of the stress correlators, from which G_{eq} is obtained, compared to the application of an external deformation which yields μ. The $T_G=0.465$ determined from the change in packing fraction lies in the middle of the rapid rise of the heat capacity. With decreasing temperature, there is a short transition period of short-term rigidity beginning near $T_{MC}=0.51$ (the end of the rise in C_P), presumably due to a lack of ergodicity, followed by the appearance of a long-term nonzero shear modulus at $T_1=0.44$ (the beginning of the rise). We believe that we have only begun to explore what shear resistance can teach us about the GT: from nonlinear mechanical properties and frequency dependences to issues related to aging.

[1] For a review, see M. Adam and D. Lairez, in *The Physical Properties of Polymeric Gels*, edited by J. P. Cohen Addad (Wiley, New York, 1996), p. 87.
[2] *Rigidity Theory and Applications*, edited by M. F. Thorpe and P. M. Duxbury (Plenum, New York, 1999).
[3] S. J. Barsky, M. Plischke, B. Joós, and Z. Zhou, Phys. Rev. E **54**, 5370 (1996).
[4] M. Plischke and B. Joós, Phys. Rev. Lett. **80**, 4907 (1998).
[5] M. Plischke, D. C. Vernon, B. Joós, and Z. Zhou, Phys. Rev. E **60**, 3129 (1999).
[6] O. Farago and Y. Kantor, Europhys. Lett. **57**, 458 (2002).
[7] C. P. Lusignan, T. H. Mourey, J. C. Wilson, and R. H. Colby, Phys. Rev. E **52**, 6271 (1995).
[8] K. Broderix, H. Löwe, P. Müller, and A. Zippelius, Europhys. Lett. **48**, 421 (1999); Phys. Rev. E **63**, 011510 (2001).
[9] D. Vernon, M. Plischke, and B. Joós, Phys. Rev. E **64**, 031505 (2001); M. Plischke, D. C. Vernon, and B. Joós, *ibid.* **67**, 011401 (2003).
[10] G. Strobl, *The Physics of Polymers* (Springer, Berlin, 1996).
[11] S. Feng and P. N. Sen,Phys. Rev. Lett. **52**, 216 (1984).
[12] J. C. Phillips, J. Non-Cryst. Solids **34**, 153 (1979).
[13] M. F. Thorpe, J. Non-Cryst. Solids **57**, 355 (1983).
[14] M. F. Thorpe, D. J. Jacobs, N. V. Chubynsky, and A. J. Rader, in *Rigidity Theory and Applications* (Ref. [2]), pp. 239–276.
[15] A. Huerta and G. G. Naumis, Phys. Lett. A **299**, 660 (2002).
[16] C. A. Angell, in *Rigidity Theory and Applications* (Ref. [2]), pp. 297–314.
[17] Y. Yilmaz, A. Erzan, and Ö. Pekcan, Eur. Phys. J. E **9**, 135 (2002).
[18] D. Long and F. Lequeux, Eur. Phys. J. E **4**, 371 (2001).
[19] R. A. Narayanan and A. Kumar, Phys. Rev. B **60**, 11859 (1999).
[20] A. Huerta and G. G. Naumis, J. Non-Cryst. Solids **329**, 100 (2003).
[21] K. J. Rao, *Structural Chemistry of Glasses* (Elsevier, Oxford, 2002).
[22] K. Binder, J. Baschnagel, and W. Paul, Prog. Polym. Sci. **28**, 115 (2003).
[23] W. Götze and L. Sjögren, Rep. Prog. Phys. **55**, 241 (1992).
[24] J. Perez, *Physique et Mécanique des Polymères Amorphes* (Technique et Documentation Lavoisier, Paris, 1992).
[25] C. A. Angell, K. L. Ngai, G. B. McKenna, P. F. McMillan, and S. W. Martin, J. Appl. Phys. **88**, 3113 (2000).
[26] K. Okun, M. Wolfgardt, J. Baschnagel, and K Binder, Macromolecules **30**, 3075 (1997); C. Bennemann, J. Baschnagel, and W. Paul, Eur. Phys. J. B **10**, 323 (1998); M. Aichele and J. Baschnagel, Eur. Phys. J. E **229**, 245 (2001).
[27] F. Varnik and K. Binder, J. Chem. Phys. **117**, 6336 (2002).
[28] R. H. Colby, Phys. Rev. E **61**, 1783 (2000).
[29] C. A. Angell, Science **267**, 1924 (1995).
[30] U. Buchenau, J. Phys.: Condens. Matter **15**, S955 (2003).
[31] P. A. Debenedetti and F. H. Sillinger, Nature (London) **410**, 259 (2001).
[32] M. D. Ediger, C. A. Angell, and S. R. Nagel, J. Phys. Chem. **100**, 13200 (1996).
[33] K. Kremer and G. S. Grest, J. Chem. Phys. **92**, 5057 (1990).
[34] C. Bennemann, J. Baschnagel, W. Paul, and K. Binder, Comput. Theor. Polym. Sci. **9**, 217 (1999); J. Baschnagel, C. Bennemann, W. Paul, and K. Binder, J. Phys.: Condens. Matter **12**, 6365 (2000).
[35] C. Bennemann, W. Paul, K. Binder, and B. Dünweg, Phys. Rev. E **57**, 843 (1998).
[36] J. Buchholz, W. Paul, F. Varnik, and K. Binder, J. Chem. Phys. **117**, 7364 (2002).
[37] C. Bennemann, W. Paul, J. Baschnagel, and K. Binder, J. Phys.: Condens. Matter **11**, 2179 (1999).
[38] M. L. Wallace and B. Joós (unpublished).
[39] M. P. Allen and D. J. Tildesley, *Computer Simulations of*

Liquids (Oxford University Press, New York, 1987).
[40] J. F.M. Lodge and D. M. Heyes, J. Chem. Soc., Faraday Trans. **93**, 437 (1997).
[41] J. F.M. Lodge and D. M. Heyes, Phys. Chem. Chem. Phys. **1**, 2119 (1999).
[42] J. K. Krüger *et al.*,Phys. Rev. Lett. **89**, 285701 (2002).
[43] C. A. Angell, J. Phys. Chem. Solids **49**, 863 (1998).
[44] M. L. Wallace and B. Joós (unpublished).
[45] K. Vollmayr-Lee, W. Kob, K. Binder, and A. Zippelius, J. Chem. Phys. **116**, 5158 (2002).
[46] Y. Gebremichael, T. B. Schrøder, F. W. Starr, and S. C. Glotzer, Phys. Rev. E **64**, 051503 (2001); R. Yamamoto and A. Onuki, *ibid.* **58**, 3515 (1998); W. Kob, C. Donati, S. J. Plimpton, P. H. Poole, and S. C. Glotzer, Phys. Rev. Lett. **79**, 2827 (1997).
[47] G. G. Naumis, Phys. Rev. B **61**, R9205 (2000).